Surfaces and Interfaces 27 (2021) 101458

Contents lists available at ScienceDirect

Surfaces and Interfaces

journal homepage: www.sciencedirect.com/journal/surfaces-and-interfaces

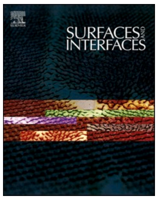

Insights toward chlorine passivation effects on electronic structures of CdTe $(\bar{1}00)$ and CdTe$(\bar{1}\bar{1}\bar{1})$ surfaces via atomistic modeling

Anthony P. Nicholson [*], Akash Shah, Aanand Thiyagarajan, Walajabad S. Sampath

Next Generation Photovoltaics Center, 1374 Campus Delivery, Fort Collins CO, 80521, U.S.A.

ARTICLE INFO

Keywords:
Cadmium telluride
Chlorine passivation
Energy band alignment
Density functional theory
Green's function
Atomistic modeling

ABSTRACT

A systematic study of varied chlorine passivation concentrations (0, 25, 50, and 100%) along Te-terminated CdTe $(\bar{1}00)$ (2×1) and CdTe$(\bar{1}\bar{1}\bar{1})(1 \times 1)$ surfaces is presented using high-fidelity atomistic computational simulations to describe the CdTe surface electronic structure. The atomistic modeling approach incorporates quantum mechanical-based calculations via density functional theory coupled with a surface Green's function formalism. Results show that fractional amounts of Cl manipulate the band alignment features of the CdTe$(\bar{1}00)$ (2×1) facet by introducing surface electronic states that bend the bands upward. The fully chlorine passivated (100%) CdTe $(\bar{1}00)$ (2×1) case reestablishes flat band conditions. As for the CdTe$(\bar{1}\bar{1}\bar{1})$ (1×1) surface, a Cl concentration of 50% mitigates upward band bending effects as well as reduces the surface electronic states present along the highly polar facet. The study also indicates that Cl concentrations of at least 50% for the CdTe$(\bar{1}00)$ and CdTe$(\bar{1}\bar{1}\bar{1})$ low-index plane orientations are necessary to decrease the CdTe electron affinity and could be used to improve band alignment found within CdTe solar cells. The investigation of Cl passivation effects on Te-terminated CdTe surfaces provides a unique atomic-scale perspective on the critical role Cl passivation has for electronic characteristics found in CdTe thin-film photovoltaic devices.

1. Introduction

Thin-film cadmium telluride (CdTe)-based photovoltaics (PV) have demonstrated significant improvements in device performance over recent years. Evidently the greatest factor enhancing CdTe PV device performance is attributed to the well-known cadmium chloride ($CdCl_2$) passivation treatment. $CdCl_2$ passivation involves the accumulation of chlorine into high energy regions containing sufficient defect densities, which primarily include grain boundaries and interfaces. In general, both grain boundaries and interfaces of thin-film CdTe PV play a critical role in the overall device performance [1]. In grain boundaries, chlorine atoms promote inversion from the p-type CdTe bulk interior to the n-type grain boundary region to enhance PV carrier collections [2,3]. Furthermore, chlorine has been determined to be the key component to suppressing electronic defects that reside within the grain boundaries by removing stacking faults [4]. Chlorine has also been reported to diffuse to CdTe-based interfaces during the annealing process [5]. However, Cl-enriched CdTe interfaces are not completely understood as these complex regions depend on several surface-dependent factors including composition, plane orientation, atomic relaxations and reconstructions. Since the $CdCl_2$ passivation treatment occurs after depositing the CdTe absorber layer, it would be worthwhile to understand the differences in surface electronic characteristics without and with Cl passivation to determine how Cl improves the overall CdTe PV device performance.

A deeper understanding of how to mitigate issues caused within the CdTe surface region is essential to maintaining and enhancing thin-film CdTe PV devices. CdTe surfaces are known to be susceptible to large surface recombination velocities, leading to performance losses in both high-quality single crystal and polycrystalline CdTe thin-films [6]. The current work computationally evaluates the effect of chlorine on Te-terminated CdTe surfaces using quantum mechanical-based atomistic modeling to determine how chlorine influences the electronic structure of CdTe surfaces. More specifically, the surface energy band alignment and associated electronic properties for low-index Te-terminated CdTe surfaces without and with chlorine are systematically studied to understand what surface mechanisms chlorine introduces that could potentially increase CdTe PV device efficiencies.

An atomic-scale perspective of important electronic characteristics found in CdTe surfaces will be presented in the current work using density functional theory (DFT) coupled with the surface Green's

---

* Corresponding author.
E-mail address: apnichol@rams.colostate.edu (A.P. Nicholson).

https://doi.org/10.1016/j.surfin.2021.101458
Received 6 May 2021; Accepted 3 September 2021

function (SGF) formalism. The underlying motivation of the work is to investigate how varied chlorine concentrations for different plane orientations and surface relaxations/reconstructions affect the electronic characteristics of CdTe surfaces. The two CdTe plane orientations under evaluation consist of the non-stoichiometric, relaxed forms of the (2×1) CdTe$(\bar{1}00)$ and (1×1) CdTe$(\bar{1}\bar{1}\bar{1})$ facets, both of which have been reported in CdTe single crystal studies [7–9]. The two CdTe plane orientations have also been determined within published literature on polycrystalline CdTe thin-films [5,10,11]. Furthermore, Cl has been found to substitute Te during the $CdCl_2$ passivation treatment process [2,12]. As such, the current study only models Cl substituting Te surface atoms for the respective CdTe$(\bar{1}00)$ and CdTe$(\bar{1}\bar{1}\bar{1})$ facets and does not consider further Cl-related complexes. Spatially-dependent energy band alignments are obtained from the DFT+SGF method for each CdTe surface at various Cl concentrations to generate further discussion on the effects Cl passivation has on CdTe PV device performance.

2. Computational details

All DFT+SGF calculations were performed on the QuantumATK Q-2019.12 software package [13,14] and follow the procedural outline used in past work [15]. The Te-terminated CdTe surfaces with varied Cl

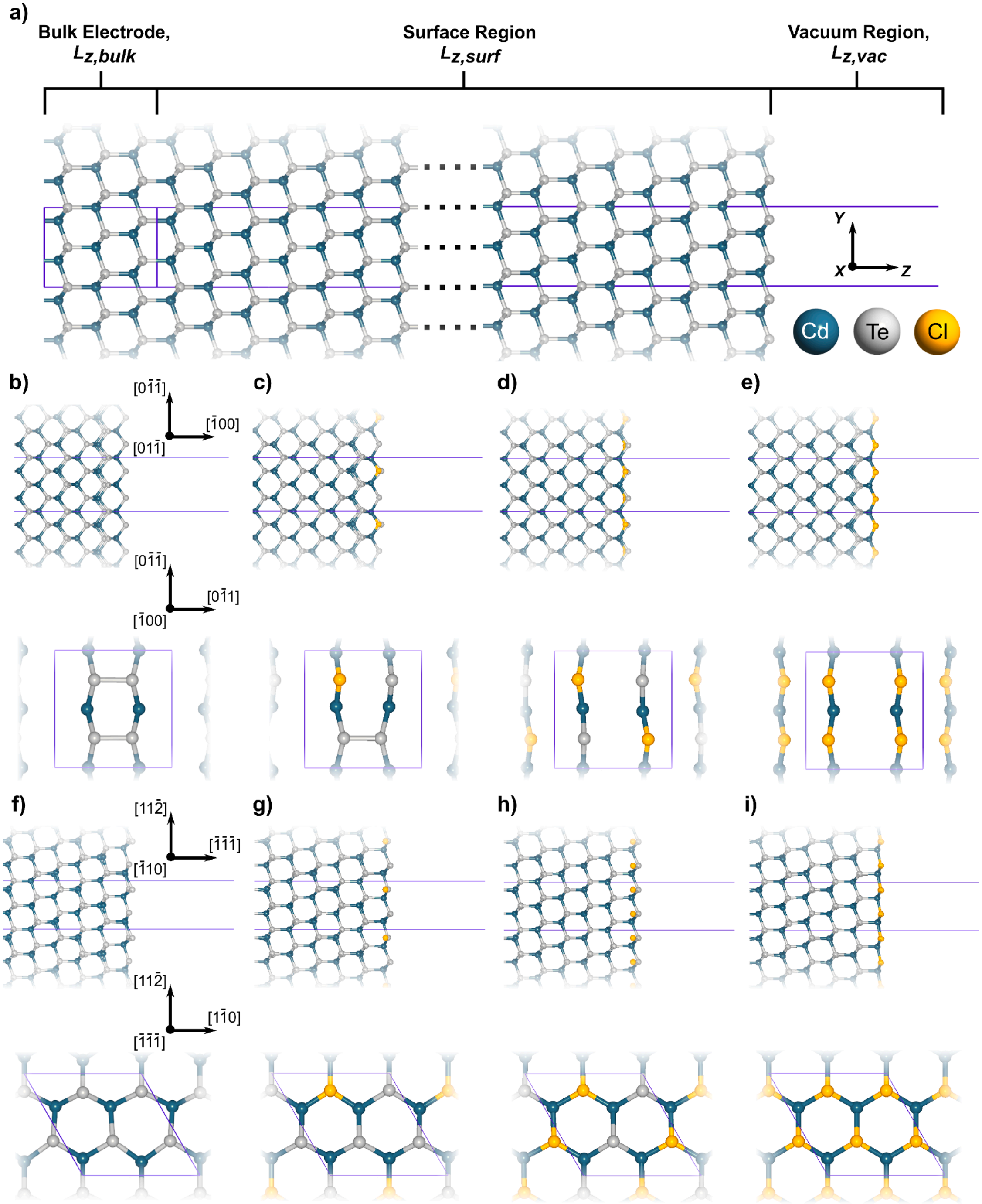

Fig. 1. (a) Schematic of general CdTe surface modeling domain using DFT and surface Green's function; (b) thru (e) depict the sideviews (top inset) and cross-sectional views (bottom inset) of the $(\bar{1}00)_{(2\times1)}$ CdTe facet with 0%, 25%, 50%, and 100% Cl, respectively; Similiarly, (f) thru (i) depict the side and cross-sectional views for the $(\bar{1}\bar{1}\bar{1})_{(1\times1)}$ CdTe facet with 0%, 25%, 50%, and 100% Cl, respectively.

concentrations were all relaxed (geometrically optimized), causing the CdTe($\bar{1}00$) facet to adopt a (2 × 1) reconstruction while the CdTe($\overline{111}$) facet remained a (1 × 1) unreconstructed surface (from hereon, the CdTe facets under investigation will have their reconstructions written in subscript form). The CdTe$(\bar{1}00)_{(2\times1)}$ model retained a Te surface coverage of 1.0 and has been verified to exist via Scanning Tunneling Microscopy [16]. All DFT computations are performed using a Linear Combination of Atomic Orbitals (LCAO) basis scheme. Each CdTe surface modeling domain consists of Cd and Te atoms using the FHI pseudopotential (PP) with a double-zeta polarized basis set and the OMX [17, 18] PP with a low(s2p2d1) basis set, respectively. The Perdew-Zunger [19] form of the LDA exchange-correlation functional was employed in all calculations. A Hubbard-U correction was applied to Cd (Cd-4d = 4.6 eV) and Te (Te-5p = 2.55 eV) to establish the proper CdTe bulk band gap value E_g of 1.49 eV as documented in the previous DFT+SGF Cd-terminated CdTe surface study [15]. The Brillouin zone is sampled by 3 × 3 × 150 (4.38 Å × 4.38 Å × 154.7 Å) and 4 × 4 × 100 (5.05 Å × 5.05 Å × 178.63 Å) for the CdTe($\bar{1}00$) and CdTe($\overline{111}$) atomistic models, respectively.

Each of the Te-terminated CdTe models maintained similar domain lengths and vacuum regions for easier comparison. A representative modeling domain for the CdTe surfaces is presented in Fig. 1a, which consists of a bulk electrode, surface region and vacuum region. The semi-infinite CdTe bulk electrode ensures that the electronic properties far away from the termination layer accurately correspond to a periodic CdTe system. The CdTe surface region is coupled to the bulk electrode by means of the Green's function formalism [20] with a large enough thickness to account for possible screening effects. Electronic features along the CdTe surface presented in the current work were determined to not change with longer modeling domains (please see the Supplementary Material for more details). The vacuum region of each CdTe surface model does not contribute to the LCAO-based calculation of the Hamiltonian matrix and thus is maintained at 5 nm simply for visual consistency. The Dirichlet and Neumann boundary conditions are implemented between the respective bulk/surface and surface/vacuum interfaces following the same procedure as previous work [15]. Only the relaxed modeling domains are presented here as they are more representative of the effects seen on epitaxial surfaces during real-world processing conditions. The respective number of atoms used in the bulk electrode and surface region of the CdTe$(\bar{1}00)_{(2\times1)}$ (CdTe$(\overline{111})_{(1\times1)}$) facet is 16 (24) and 528 (480). The bulk electrode size was set as 6.48 Å(11.22 Å). The eight relaxed CdTe surface models used in the study are illustrated in Figs. 1b thru 1i. A force threshold of 0.01 eV/Å was applied to the last 5 nm of the surface region while all other atoms were fixed in each CdTe surface model. All investigated surface supercell sizes after relaxation are provided in Table 1.

3. Results and discussion

The resulting electronic structures of CdTe surfaces with varied concentrations of Cl passivation are evaluated according to their respective CdTe$(\bar{1}00)_{(2\times1)}$ and CdTe$(\overline{111})_{(1\times1)}$ facets. A detailed description of energy band alignment and surface electronic states associated with passivation and relaxation effects is presented below.

Table 1
CdTe one-probe modeling dimensions of the relaxed surface regions with respect to Cl passivation on the surface for the CdTe$(\bar{1}00)_{(2\times1)}$ and CdTe$(\overline{111})_{(1\times1)}$ facets.

CdTe Facet	$Cl_{Te,surf}$	$L_{z,surf}$ (Å)
$(\bar{1}00)_{(2\times1)}$	0%	213.52
	25%	213.65
	50%	213.52
	100%	213.3
$(\overline{111})_{(1\times1)}$	0%	223.88
	25%	223.85
	50%	223.86
	100%	223.6

3.1. *Cl passivation along CdTe$(\bar{1}00)_{(2\times1)}$ facet*

Fig. 2 depicts the energy band alignments at different Cl surface concentrations for the CdTe$(\bar{1}00)_{(2\times1)}$ surface configuration. The magnitudes of electronic features associated with the band alignments are provided in Table 2. In general, the calculated band gaps ($E_{g,CdTe}$) after applying the Hubbard U correction are in good agreement with the expected value of 1.5 eV since for single crystal CdTe the band gap can vary down to as low as 1.41 eV with temperature changes [21]. Establishing an appropriate CdTe bulk band gap enables a more quantitative representation of the measured energy levels of each band alignment plot.

The original CdTe surface without Cl (0% Cl_{Te}, Fig. 2a) contains minimal band bending effects and thus retains flattened conduction and valence bands across the entire length of the modeling domain. The energetically favorable atomic (2 × 1) reconstruction that involves Te atoms forming dimers as seen in Fig. 1b is responsible for the flat band condition and satisfies the electron counting rule [22]. The relaxed CdTe $(\bar{1}00)_{(2\times1)}$ surface is found to be one of the experimentally stable reconstructed surfaces forming within an excess Te flux and evaporation temperatures exceeding 300–340 °C [23–25]. The stable configuration predicted by the DFT+SGF method after geometry optimization for CdTe($\bar{1}00$) is indeed the (2 × 1) reconstruction and has been reported in past DFT calculations [8].

As the Cl concentration increases to 25% and 50% (Fig. 2b and Fig. 2c), a noticeable upward band bending effect of at least 0.5 eV occurs in both the valence and conduction bands of the CdTe surface. The band bending is due to a negative charging effect that results from charge rearrangement at the surface (please see the Supplementary Material for verification using the Mulliken population analysis). The negative charge is induced by both the surface relaxation and passivation by Cl, which due to its lower valence than Te would cause a surface charge imbalance. As the CdTe($\bar{1}00$) facet contains only two bonds per surface atom, substituting Te with Cl at fractional amounts disrupts the charge balance that was initially maintained as seen for the (2 × 1) reconstruction. The surface cross-sectional views of the 25% and 50% Cl_{Te} passivated CdTe($\bar{1}00$) facets as depicted in Figs. 1c and 1d do not form a dimer to neutralize the dangling bonds, which as a result causes a negative charge along the CdTe($\bar{1}00$) surface. In turn, the negatively charged surfaces due to fractional amounts for Cl passivation force the bands to bend upward with a large screening length. It is noted that no immediate cusp feature develops within the valence band edge. Instead, only a visible plateau forms for the 50% case that is most likely due to the atomic relaxation that induces strain-dependent changes to the valence band within that region.

When the CdTe($\bar{1}00$) surface experiences complete Cl passivation (Fig. 2d), the band bending effect is removed from the band alignment and now includes a small additional cusp potential seen 63.45 Å away from the surface ($L_{z,\mathrm{surf}}$ - $\delta_{\mathrm{v,cusp}}$ = 63.45 Å). A similar cusp feature has been reported in the earlier study for Cd-terminated CdTe surfaces [15] and is directly attributed to the relaxation applied to the model. The cusp may offer an additional driving force for hole charge carriers to move toward the CdTe surface but is not expected to make significant improvements to device performance. In a similar manner as the bare (0% Cl_{Te}) CdTe($\bar{1}00$) (2 × 1) facet, the 100% Cl_{Te} covered CdTe($\bar{1}00$) surface forms dimers that mitigate the presence of dangling bonds. As a result, both the 0% and 100% Cl_{Te} CdTe$(\bar{1}00)_{(2\times1)}$ surfaces demonstrate minimal surface electronic states and flattened valence/conduction bands throughout the modeling domain.

Further details of how the surface atoms contribute to the band

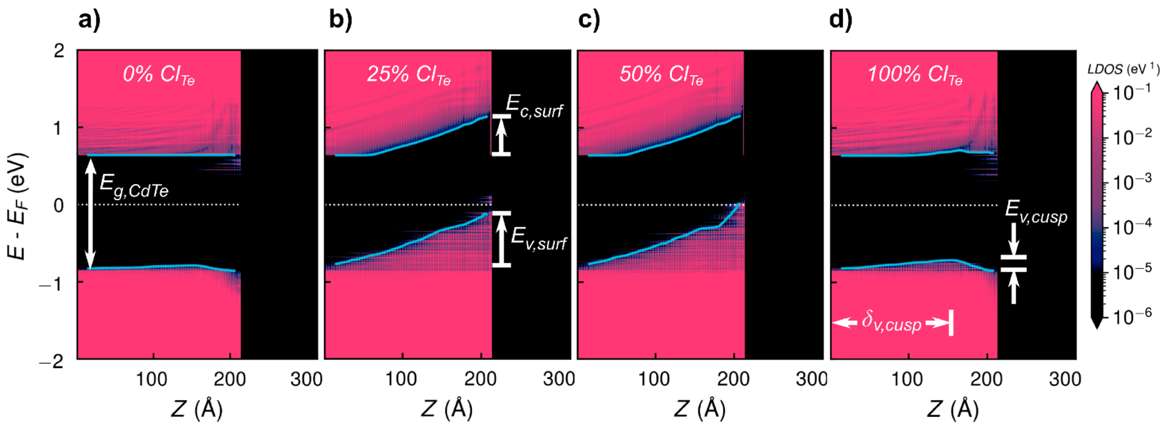

Fig. 2. Localized density of states mapping for the CdTe($\bar{1}00$)$_{(2\times1)}$ one-probe models with Cl_{Te} passivating concentrations of (a) 0%, (b) 25%, (c) 50%, and (d) 100%. The pink regions indicate high density of states while black regions represent negligible density of states. The zero energy on the y-axis is referenced by the Fermi level E_F of each respective band alignment profile. The light blue curves are the macroscopically averaged curve fits of the valence band maximum and conduction band minimum, respectively. (For interpretation of the references to colour in this figure legend, the reader is referred to the web version of this article.)

Table 2
Quantified electronic band alignment features for each Cl_{Te}-concentration along the CdTe($\bar{1}00$)$_{(2\times1)}$ one-probe surface model. $\delta_{v,cusp}$ indicates the position where any internal cusp energy potentials $E_{v,cusp}$ are determined within the surface band alignment plot. All energy band alignment values are obtained from the macroscopically averaged curve fit of each local density of states plot. Any +/- values indicate energy values referenced to the Fermi level E_F (marked as 0 eV).

Cl_{Te} Conc. (%)	0	25	50	100
$E_{g,CdTe}$ (eV)	1.47	1.41	1.41	1.46
$E_{c,surf}$ (eV)	0	+0.5	+0.51	+0.03
$E_{v,surf}$ (eV)	-0.03	+0.64	+0.78	-0.03
$\delta_{v,cusp}$ (Å)	133.65	N/A	N/A	149.85
$E_{v,cusp}$ (eV)	+0.04	N/A	N/A	+0.1

alignment features is provided in Fig. 3 using a projected device density of states (PDDOS) analysis. The p-orbital contribution of surface electronic states for the given surface atoms of each CdTe($\bar{1}00$) model provides a way to specifically identify which element contributes most to the surface band alignment features. Each PDDOS plot includes the respective bulk $E_{v,bulk}$ and $E_{c,bulk}$ energy levels to more clearly see how far within the CdTe bulk band gap the surface electonic states extend. It must be noted that the electronic states may reside within the surface conduction and valence bands but still heavily contribute to the band bending features present for a given CdTe modeling case.

Fig. 3a reveals how the unpassivated Te surface atoms do not introduce any surface electronic states between the valence and conduction band energy levels of bulk CdTe. This confirms that the charge is balanced along the surface, leading to a flat band alignment for the bare CdTe($\bar{1}00$) facet. A CdTe($\bar{1}00$)$_{(2\times1)}$ facet with Te only at the surface demonstrates clean band alignment features due to the reconstruction eliminating dangling bonds and thus maintaining surface charge neutrality.

The 25% and 50% covered CdTe($\bar{1}00$) facets as shown in Figs. 3b and 3c, on the other hand, show a noticeable presence of surface electronic states between $E_{v,bulk}$ and $E_{c,bulk}$ energy levels. More specifically, the q_1 and q_3 Te atoms are the dominant atoms inducing the upward band bending seen in Figs. 2b and 2c. The Cl atom located at q_2 is, however, only mildly affecting the electronic states. Nonetheless, the presence of Cl in fractional amounts causes a noticeable charge accumulation along some of the Te surface atoms that induce the presence of surface electronic states. Clearly, higher concentrations of Cl passivation affect energy band alignement in a manner that could readily impact CdTe PV device charge transport.

The CdTe($\bar{1}00$)$_{(2\times1)}$ DFT+SGF atomistic models with fractional amounts of Cl surface concentrations introduce pronounced band alignment characteristics in comparison to the bare and fully Cl covered surface models. The large band bending in such models could be advantageous as long as the features were retained after forming an interface with another layer on top of CdTe. For example, the minority charge carriers (electrons) in the conduction band would be impeded from flowing across the junction due to the upward band bending acting as a barrier. On the other hand, the majority charge carriers (holes) in the valence band would easily transport across the junction as the upward band bend enhances the driving force for holes to move in a certain direction. The downside of the 25% and 50% Cl_{Te} cases is their undesirable quantities of surface electronic states that would lead to recombination losses at the formed junction.

Although the bare and fully Cl-passivated CdTe($\bar{1}00$) facet models do not include band bending effects, there are minimal surface electronic states for these two models. Both the flat-band conditions and minimal surface electronic states in the 0% and 100% cases of CdTe($\bar{1}00$) is ideal for minimal recombination velocity at the back of the CdTe PV device. Flat energy bands with virtually no dangling bonds as provided by both cases would be beneficial for CdTe PV device performance as long as such benign electronic features were retained after subsequent interfacial formation at the back of the CdTe absorber layer. However, further DFT+GF interfacial modeling would be necessary as the surface electronic features would change depending on what overlayer is deposited on the CdTe($\bar{1}00$) facet, which is beyond the scope of the present discussion.

3.2. Cl passivation along CdTe($\overline{111}$)$_{(1\times1)}$ facet

The Cl passivation effect on the CdTe($\overline{111}$) oriented surfaces is presented in Fig. 4. All pertinent energy values within the energy band alignment plots are recorded in Table 3. As seen in the CdTe($\bar{1}00$) cases, the measured band gap in the bulk region of each CdTe($\overline{111}$) model was in relatively good agreement with the experimental value for $E_{g,CdTe}$.

The initially bare CdTe($\overline{111}$)$_{(1\times1)}$ unreconstructed surface (Fig. 4a) exhibits highly polar characteristics leading to large upward band bending with magnitudes of +0.44 eV and +0.74 eV for $E_{c,surf}$ and $E_{v,surf}$, respectively. Structurally, there are small changes to the surface arrangement with the surface atoms being slightly displaced from their original positions (Fig. 1f). Secondly, since the ($\overline{111}$) plane orientation contains three bonds per Te surface atom, it is often stated that dangling

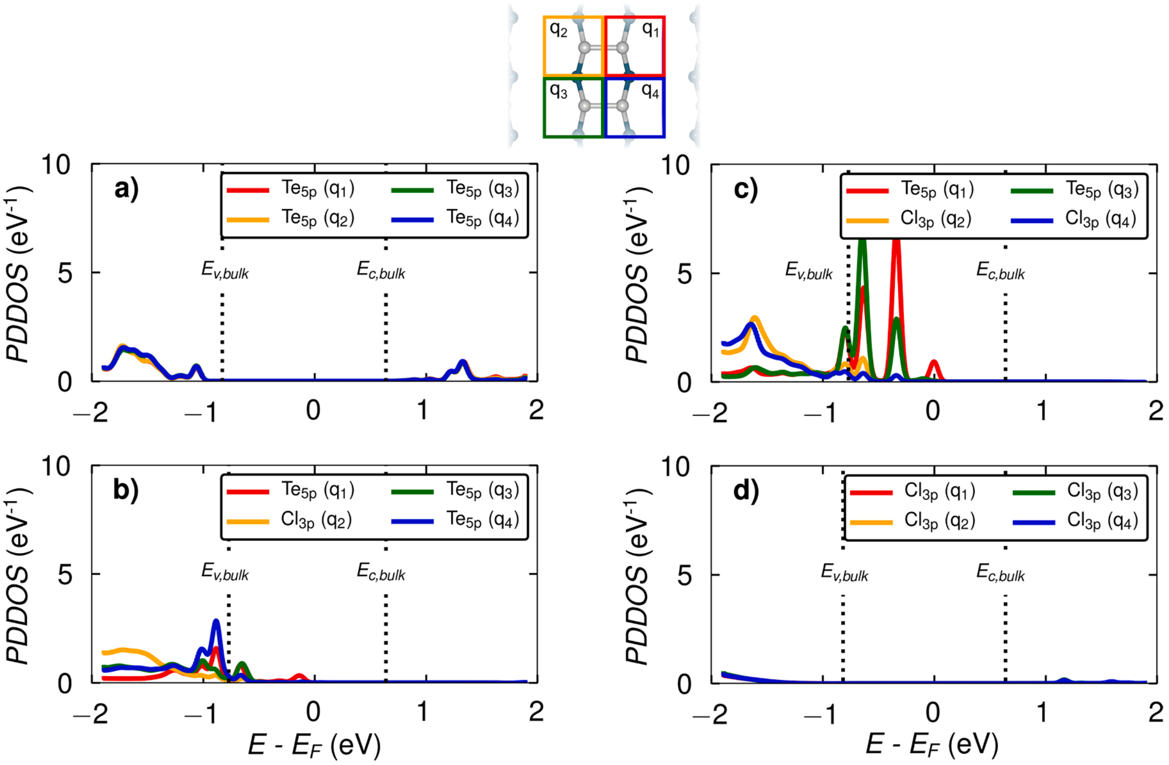

Fig. 3. Projected device density of states (PDDOS) of the termination surface atoms for the CdTe$(\overline{1}00)_{(2\times1)}$ facet with (a) 0%, (b) 25%, (c) 50%, and (d) 100% Cl_{Te} passivation. Each surface atom is labeled according to the cross-sectional quadrant position that it occupies as indicated in the top inset image. The valence and conduction band energy levels of the CdTe bulk region ($E_{\mathrm{v,bulk}}$ and $E_{\mathrm{c,bulk}}$) are labeled along their respective dotted lines. Only the p-orbital contribution of each surface atom is shown. A gaussian width of 0.05 eV was used for all PDDOS curves.

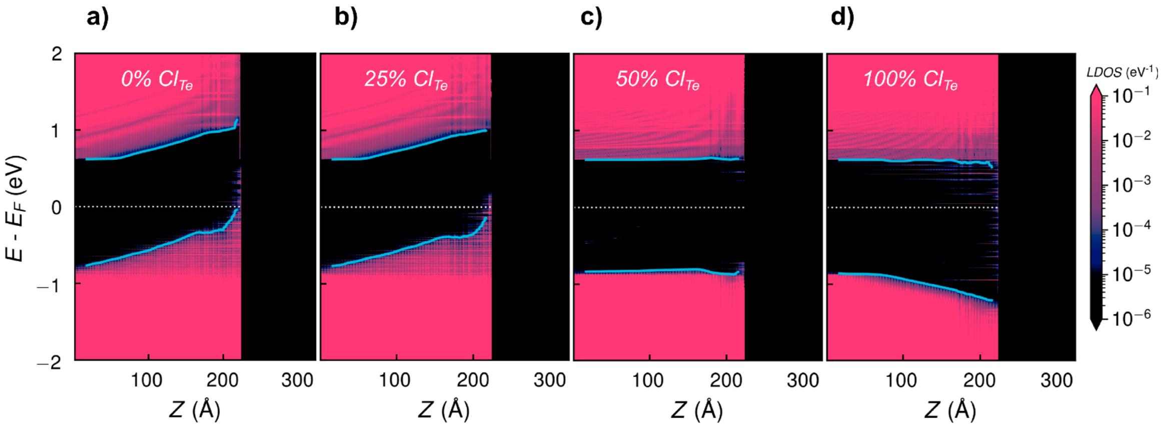

Fig. 4. Localized density of states mapping for the CdTe$(\overline{1}\overline{1}\overline{1})_{(1\times1)}$ one-probe models with Cl_{Te} passivating concentrations of (a) 0%, (b) 25%, (c) 50%, and (d) 100%. The pink regions indicate high density of states while black regions represent negligible density of states. The zero energy on the y-axis is referenced by the Fermi level E_F of each respective band alignment profile. The light blue curves are the macroscopically averaged curve fits of the valence band maximum and conduction band minimum, respectively. (For interpretation of the references to colour in this figure legend, the reader is referred to the web version of this article.)

bond formation is likely to occur since each Te suface atom is no longer tetrahedrally coordinated. As a result, the dangling bonds induce the negative surface charging responsible for the upward bend in the CdTe$(\overline{1}\overline{1}\overline{1})_{(1\times1)}$ surface model with no Cl_{Te} coverage.

In the 25% Cl_{Te} coverage CdTe$(\overline{1}\overline{1}\overline{1})_{(1\times1)}$ model (Fig. 4b), the upward band bending is retained but there is a noticeable decrease in surface states present. The values for $E_{\mathrm{c,surf}}$ and $E_{\mathrm{v,surf}}$ have also decreased by at least 0.07 eV in comparison to the bare CdTe$(\overline{1}\overline{1}\overline{1})$ case. Although the difference is minor, the addition of Cl at the CdTe surface tends to redistribute the charge and thus mitigate some of the deleterious effects caused by the Te-terminated CdTe$(\overline{1}\overline{1}\overline{1})_{(1\times1)}$ surface (please see the Supplementary Material for how chlorine slightly reduces the negative charging in the 25% Cl_{Te}-passivated CdTe$(\overline{1}\overline{1}\overline{1})_{(1\times1)}$ case according to the Mulliken population analysis). Interestingly, both models still contain a cusp-like feature in the valence band.

As 50% Cl_{Te} coverage is achieved (Fig. 4c), there is a clear indication that the net surface charge is minimized due to the presence of Cl. As a result, the bands are significantly flatter than seen for the previous two CdTe$(\overline{1}\overline{1}\overline{1})$ cases. Visually, there are few electronic states present with such states exhibiting lower DOS magnitudes. Apparently the half-

Table 3
Quantified electronic band alignment features for each Cl_{Te}-concentration along the CdTe$(\overline{111})_{(1\times1)}$ one-probe surface model. $\delta_{v,cusp}$ indicates the position where any internal cusp energy potentials $E_{v,cusp}$ are determined within the surface band alignment plot. All energy band alignment values are obtained from the macroscopically averaged curve fit of each local density of states plot. Any +/- values indicate energy values referenced to the Fermi level E_F (marked as 0 eV).

Cl_{Te} Conc. (%)	0	25	50	100
$E_{g,CdTe}$ (eV)	1.39	1.39	1.46	1.48
$E_{c,surf}$ (eV)	+0.44	+0.37	+0.01	-0.1
$E_{v,surf}$ (eV)	+0.74	+0.63	-0.01	-0.35
$\delta_{v,cusp}$ (Å)	163.21	162.28	143.57	N/A
$E_{v,cusp}$ (eV)	+0.43	+0.38	+0.03	N/A

passivated CdTe$(\overline{111})$ surface with Cl removes most of the charging effects initially found on the highly polar facet while maintaining a lower density of defect states. The 50% Cl_{Te}-passivated CdTe$(\overline{111})_{(1\times1)}$ surface may prove to be the most advantageous in terms of favorable band alignment conditions.

For the fully Cl-passivated CdTe$(\overline{111})_{(1\times1)}$ surface (Fig. 4d), the valence band begins to bend downward by a magnitude of 0.35 eV and several surface states appear throughout the surface band gap region. Despite the 5 nm surface region undergoing geometry optimization during the DFT+SGF methodology, there is no presence of a cusp energy potential. There are clear differences between the CdTe$(\overline{111})$ Te-terminated surface and the fully Cl-passivated surface as the former bends the bands upward while the latter bends the valence band downward. It is evident that having a lower valence element acting as the CdTe$(\overline{111})$ surface termination layer can cause drastic changes to the band alignment properties that are not seen in the similar comparison between the CdTe$(\bar{1}00)$ 0% and 100% Cl_{Te} coverage cases.

The PDDOS of each surface atom for the CdTe$(\overline{111})_{(1\times1)}$ facet models are evaluated in Fig. 5. The 0% Cl_{Te} case in Fig. 5a clearly shows how all 5p orbitals of the Te surface atoms are contributing to the electronic states that induce the upward band bending seen in Fig. 4a. Accordingly, the Te surface atoms are negatively charging due to the dangling bond formation after cleaving CdTe along the $(\overline{111})$ plane. Yet for the 25% case (Fig. 5b), there is a significant decrease in the PDDOS level and indicates that the single Cl surface atom reduces the number of electronic states residing on the other Te surface atoms. Nonetheless, there is still large band bending effects for this case and suggests that the residual surface charge still can cause significant effects to surface band alignment.

In contrast, the 50% Cl_{Te} CdTe$(\overline{111})$ case no longer develops any surface states between the valence and conduction band edges, which is confirmed by the minimal states found within the band alignment of Fig. 4c. Thus there is clear evidence that the charge is minimized on the surface due to the increased Cl concentration.

The surface states are not visible in Fig. 5d for the 100% Cl_{Te} case although the band alignment (Fig. 4d) shows otherwise. Using a gaussian width of 0.05 eV tends to smear out the PDDOS peaks that only extend for ±5 meV for the 100% Cl_{Te} CdTe$(\overline{111})$ model, which is why it appears as if no surface electronic states exist on this surface (please see Supplementary Material for comparison of PDDOS plots with lower gaussian widths). The greatest electronic state is found at 0.61 eV but is simply confined to that energy level as opposed to the more prominent peaks found in the bare CdTe$(\overline{111})_{(1\times1)}$ model. It has been verified that the immediate layer beneath the Cl_{Te} termination layer, which consists only of cadmium atoms, actually contributes the most to the surface electronic states present for this case. Further discussion on the surface electronic states of the 100% Cl_{Te} CdTe$(\overline{111})$ surface model can be found in the Supplementary Materials.

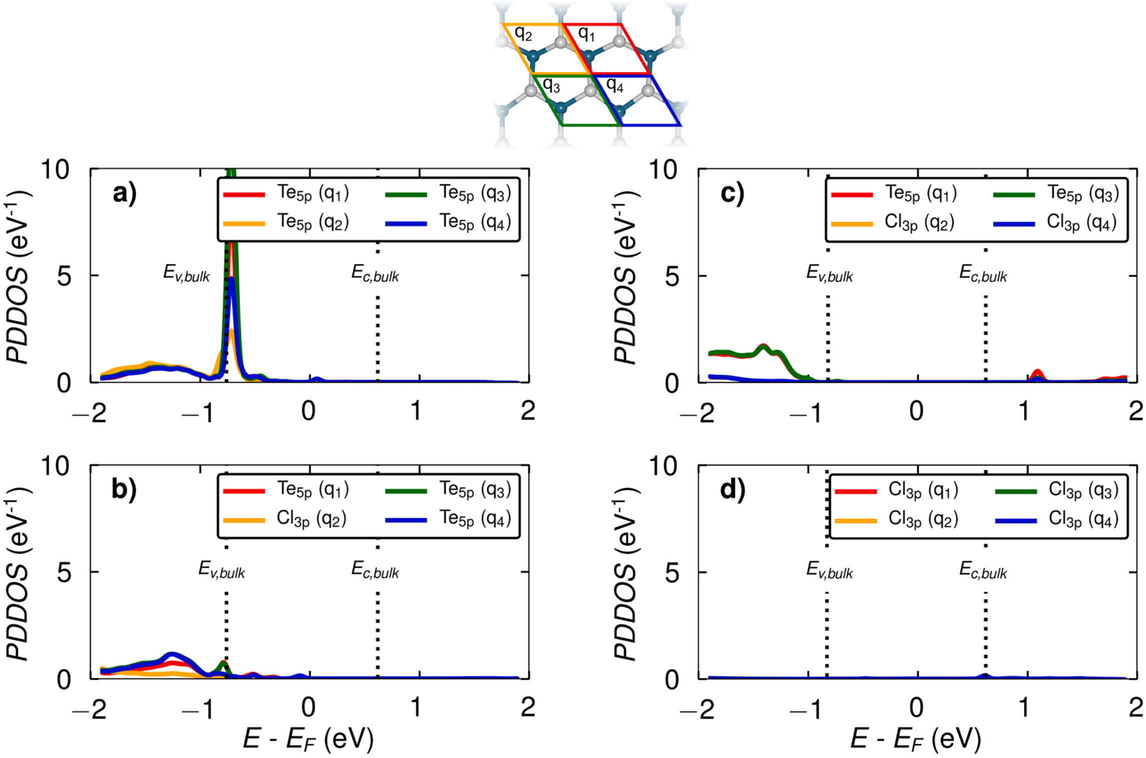

Fig. 5. Projected device density of states (PDDOS) of the termination surface atoms for the CdTe$(\overline{111})_{(1\times1)}$ facet with (a) 0%, (b) 25%, (c) 50%, and (d) 100% Cl_{Te} passivation. Each surface atom is labeled according to the cross-sectional quadrant position that it occupies as indicated in the top inset image. The valence and conduction band energy levels of the CdTe bulk region ($E_{v,bulk}$ and $E_{c,bulk}$) are labeled along their respective dotted lines. Only the p-orbital contribution of each surface atom is shown. A gaussian width of 0.05 eV was used for all PDDOS curves.

It has been suggested from outside literature [26] that CdTe epitaxial growth process occurs in the $\langle\overline{111}\rangle$ direction, making the varied Cl-passivation cases worthwhile to evaluate altogether. In general, lower Cl concentrations (0% and 25% cases) tend to create large upward band bending effects that are primarily due to negative charge build-up on the surface induced by dangling bonds. Although upward band bending is generally beneficial for selective charge transport toward the back of a p-type CdTe absorber layer, the high magnitudes of surface electronic states would cause large amounts of recombination at these surfaces. In turn, the overall CdTe PV device efficiency would suffer if the predicted band alignment features in either the 0% or 25% $\mathrm{Cl_{Te}}$ $\mathrm{CdTe}(\overline{111})_{(1\times1)}$ surface still existed after forming an interface with a deposited overlayer.

It is not until upon reaching a Cl-passivating surface concentration of 50% that the $\mathrm{CdTe}(\overline{111})$ band alignment flattens out due to minimized charging on the surface from the reduction of electronic states. It is reasonable to believe that the 50% $\mathrm{Cl_{Te}}$ $\mathrm{CdTe}(\overline{111})_{(1\times1)}$ surface would perform exceptionally well due a lowered surface recombination velocity as there is minimal surface charging present. As a result, the charge transport of majority and minority carriers near the CdTe surface region would not be impeded as the band alignment provided by this surface is flat in comparison to the other cases, maintaining higher CdTe device efficiencies. On the other hand, completely passivating the $\mathrm{CdTe}(\overline{111})_{(1\times1)}$ surface with Cl introduces more surfaces states that would increase recombination velocities in comparison to the 50% case (albeit with low DOS magnitudes). The downward band bending in the 100% $\mathrm{Cl_{Te}}$ case also prevents majority hole charge carriers from being transported toward the back of the thin-film CdTe solar cell and would thus decrease the solar cell efficiency. Controlling the Cl passivation along the $\mathrm{CdTe}(\overline{111})_{(1\times1)}$ facet to achieve a concentration of 50% may optimize the band alignment characteristics of the $\mathrm{CdTe}(\overline{111})$ surface that may be better for interfacial band alignment between the CdTe layer and deposited overlayer.

Overall, the amount of surface passivation that the CdTe surface undergoes after the CdTe epitaxial growth process will evidently influence the charge transport behaviors within CdTe PV devices. The complexity of energy band alignment is expected to increase for polycrystalline CdTe thin-films since they obviously contain a number of preferred plane orientations and possible intrinsic defects existing at the surface. Furthermore, the current DFT+SGF method is incapable of predicting the influence of annealing on the surface characteristics of polar Te-terminated CdTe surfaces, which has been experimentally researched in the past [25,27]. In any case, the energy band alignment predicted by the DFT+SGF method does provide a succinct overview of how chlorine passivation, in combination with preferred plane orientations, relaxation effects, and surface reconstructions, affects CdTe surface band alignment in ways that it can be tailored for optimized CdTe PV device performance.

3.3. *Calculated electron affinities of CdTe surfaces*

A systematic determination of the electron affinity for CdTe surfaces is necessary to distinguish how various surface conditions influence band alignment during interfacial formation. The electron affinity is defined as the energy required to remove an electron from the bottom of the conduction band at the surface to the local vacuum level [28], which is dependent upon the electric potential difference formation at the surface of the semiconductor. Furthermore, it is known that variations in electron affinity due to plane orientation and surface reconstruction are likely to occur as well [29]. In crystalline materials, the orientation and the structure of the surface is known to affect the surface charge rearrangement, leading to surface-dependent electronic properties [30] that influence the electron affinity. A similar effect has been reported within surface modification studies of CdTe surfaces [31]. However, no previous studies have evaluated a combination of relaxation and reconstution effects along with how Cl concentrations modify the CdTe electron affinity. Therefore, it becomes imperative to understand from an atomistic perspective how the Te-terminated CdTe surfaces with varied $\mathrm{Cl_{Te}}$-passivation levels are affecting the electron affinity. The following equation describes the method for calculating electron affinity using the SGF method:

$$\chi = -W_{SGF} - \Delta E_{C,F} - E_{c,surf} \tag{1}$$

where W_{SGF} is a calculated energy level referenced from the chemical potential (intrinsic Fermi level of semiconductor) to vacuum, $\Delta E_{C,F}$ is the energy difference between the Fermi energy position and the conduction band level in the bulk, and $E_{\mathrm{c,surf}}$ is surface potential measured in Sections 3.1 and 3.2. Fig. 6 illustrates the aforementioned band alignment parameters used to calculate electron affinity χ for each Te-terminated CdTe atomistic model. The calculated energy level W_{SGF} uses a similar notation as the work function of metals found by the SGF method [20] and is generally defined for a semiconductor as follows:

$$W_{SGF} = -e\left\langle \delta V_E \right\rangle^{vac} - E_F^{bulk} \tag{2}$$

where e is electron charge, $\langle \delta V_E \rangle^{vac}$ is the macroscopically averaged electrostatic difference potential, and $E_{\mathrm{F}}^{\mathrm{bulk}}$ is the Fermi level. An example of the electrostatic difference potential for the 0% $\mathrm{Cl_{Te}}$ $\mathrm{CdTe}(\overline{111})_{(1\times1)}$ facet using the SGF method is found in Fig. 6. The electron affinity dependence on surface features are provided in Table 4.

In general, all calculated electron affinity magnitudes lie outside the typical range of experimental values (4.28 eV to 4.5 eV) found for CdTe [21]. It is also often accepted in outside device numerical modeling studies on CdTe-based PV to use electron affinity values that lie between 3.9 to 4.4 eV [32,33]. However, there is no indication as to how the electron affinity changes with varied species along the termination layer in any of these studies. As a brief example, the Cd-terminated CdTe $(111)_{(1\times1)}$ surface from a previous DFT+SGF study [15] gives $\chi = 4.13$ eV using Eq. (1) and thus is much closer to the experimental value than the Te-terminated cases. This could be an indication that the Te-terminated CdTe surfaces may not be the preferential termination layer for band alignment. Nonetheless, it is clear that Cl passivation does dramatically influence the CdTe electron affinity and could be used to provide better band alignments during the $\mathrm{CdCl_2}$ passivation treatment process. The following discussion gives a qualitative description of the Cl passivation effect for both the $(\overline{1}00)$ and $(\overline{111})$ CdTe cases.

By focusing more on the relative differences between the calculated parameters, we see that there is less variation in the electron affinity for the $(\overline{1}00)$ cases as opposed to the $(\overline{111})$ CdTe surfaces. Starting with the $(\overline{1}00)$ cases, Cl concentrations from 0% to 50% are relatively consistent with each other. However, using 100% $\mathrm{Cl_{Te}}$ on the CdTe surface decreases the magnitude by 1.89 eV in comparison to the bare CdTe $(\overline{1}00)_{(2\times1)}$ facet. The $\mathrm{CdTe}(\overline{111})$ cases show a more consistent decreasing trend in the CdTe electron affinity with higher $\mathrm{Cl_{Te}}$ passivation. The bare (0% $\mathrm{Cl_{Te}}$) $\mathrm{CdTe}(\overline{111})$ facet has the highest predicted electron affinity magnitude despite the large upward band bending feature in the surface band alignment. The electron affinity continues to drop with additional amounts of Cl passivation upon reaching the lowest magnitude of 2.44 eV.

It is reasonable to assume that a passivation value somewhere between 50% and 100% could effectively achieve a value that falls between the range of expected CdTe electron affinities for the plane orientations and surface reconstructions used in this study. Secondly, both the $\mathrm{CdTe}(\overline{1}00)_{(2\times1)}$ and $\mathrm{CdTe}(\overline{111})_{(1\times1)}$ facets tend to have their electron affinities decrease for $\mathrm{Cl_{Te}}$ passivating concentrations between 50% to 100%. Both results indicate that Cl passivation may offer a way to control the CdTe electron affinities in a manner that is more desirable for interfacial band alignment. Lower CdTe electron affinities may lead

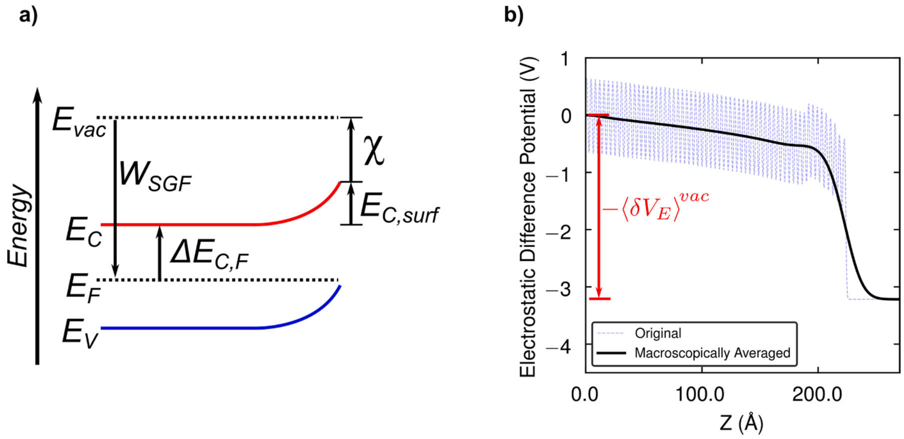

Fig. 6. (a) Schematic representation of the band alignment parameters used to calculate electron affinity χ. Note that the downward and upward pointing directions of arrows denote a negative and positive energy value, respectively, along the energy scale; (b) Example of the macroscopically averaged electrostatic difference potential $-e\langle\delta V_E\rangle^{vac}$ used for calculating W_{SGF} along the CdTe$(\overline{111})_{(1\times1)}$ facet.

Table 4
Surface-dependent chemical potential reference level W_{SGF} and electron affinity χ_{CdTe} calculated for the Te-terminated CdTe$(\overline{1}00)$ and CdTe$(\overline{111})$ surfaces at varied Cl_{Te} passivation concentrations.

Facet	Cl_{Te} conc. (%)	W_{SGF} (eV)	χ (eV)
$(\overline{1}00)_{(2\times1)}$	0%	-6.02	5.38
	25%	-6.71	5.57
	50%	-6.49	5.34
	100%	-4.1	3.49
$(\overline{111})_{(1\times1)}$	0%	-7.16	6.1
	25%	-6.69	5.7
	50%	-5.48	4.85
	100%	-2.96	2.44

to more favorable band alignment formations with work function values seen in metal back contacts. As a result, a greater selection of back contacts that avoid Schottky barrier formation (a major problem residing at the CdTe/back contact junction when using a metal to form an ohmic contact with the CdTe absorber layer [21,34]) may be available due to modification of the CdTe electron affinity.

4. Conclusion

The investigation of Cl passivation on Te-terminated CdTe surfaces using the DFT+SGF computational method reveals the underlying effects of plane orientation, surface relaxation/reconstruction, and Cl concentration on energy band alignment. Both the polar CdTe$(\overline{1}00)$ and CdTe$(\overline{111})$ facets with varying Cl_{Te} concentration were evaluated for any key differences and features present in the surface energy band alignments of the CdTe surface models. The bare and fully passivated (0% and 100%, respectively) CdTe$(\overline{1}00)_{(2\times1)}$ as well as the 50% CdTe$(\overline{111})_{(1\times1)}$ facets demonstrated flattened band alignments that are a result of charge redistribution that minimizes dangling bond formation along each surface. All other facets contained notable surface band bending effects with surface electronic states that could potentially lead to higher surface recombination velocity and thus compromise CdTe PV device performance. Secondly, the calculated electron affinities for each of the Cl passivated CdTe surfaces indicate that higher Cl concentrations ($50\% \leq x \leq 100\%$) will decrease the electron affinity magnitude and could be useful for controlling the energy band alignment formation when a back contact is deposited on CdTe. The atomistic modeling approach for calculating energy band alignment in Cl_{Te}-passivated CdTe surfaces provides a fundamental and widely encompassing perspective of how specific chlorine concentrations enhance the CdTe surface electronic structures and thus contribute to the improvement of CdTe thin-film PV device performance.

Declaration of Competing Interest

The authors declare that they have no known competing financial interests or personal relationships that could have appeared to influence the work reported in this paper.

Acknowledgements

The authors would like to thank Umberto Martinez for his assistance and expertise on using the QuantumATK modeling framework within the current study. This material is based upon work supported by the National Science Foundation Graduate Research Fellowship Program under Grant No. DGE-1321845, INTERN Program under Grant No. 1540007, and Industry-University Cooperative Research Centers Program under Grant No. 1821526. Any opinions, findings, and conclusions or recommendations expressed in this material are those of the author(s) and do not necessarily reflect the views of the National Science Foundation. This work utilized the Summit supercomputer, which is supported by the National Science Foundation (awards ACI-1532235 and ACI-1532236), the University of Colorado Boulder, and Colorado State University. The Summit supercomputer is a joint effort of the University of Colorado Boulder and Colorado State University.

Supplementary materials

Supplementary material associated with this article can be found, in the online version, at doi:10.1016/j.surfin.2021.101458.

References

[1] A. Kanevce, M. Reese, T. Barnes, S. Jensen, W. Metzger, The roles of carrier concentration and interface, bulk, and grain-boundary recombination for 25% efficient CdTe solar cells, J. Appl. Phys. 121 (2017) 214506, https://doi.org/10.1063/1.4984320.

[2] C. Li, Y. Wu, J. Poplawsky, T.J. Pennycook, N. Paudel, W. Yin, S.J. Haigh, M. P. Oxley, A.R. Lupini, M. Al-Jassim, S.J. Pennycook, Y. Yan, Grain-boundary-enhanced carrier collection in CdTe solar cells, Phys. Rev. Lett. 112 (2014) 156103, https://doi.org/10.1103/PhysRevLett.112.156103.

[3] O. Zywitzki, T. Modes, H. Morgner, C. Metzner, B. Siepchen, B. Späth, C. Drost, V. Krishnakumar, S. Frauenstein, Effect of chlorine activation treatment on electron beam induced current signal distribution of cadmium telluride thin film solar cells, J. Appl. Phys. 114 (16) (2013) 163518, https://doi.org/10.1063/1.4827204.

[4] Peter Hatton, Michael Watts, Ali Abbas, John Walls, Roger Smith, Pooja Goddard, Chlorine activated stacking fault removal mechanism in thin film CdTe solar cells: the missing piece, Nat. Commun. 12 (2021), 4938, https://doi.org/10.1038/s41467-021-25063-y.

[5] A. Abbas, G.D. West, J.W. Bowers, P. Isherwood, P.M. Kaminski, B. Maniscalco, P. Rowley, J.M. Walls, K. Barricklow, W.S. Sampath, K.L. Barth, The effect of cadmium chloride treatment on close spaced sublimated cadmium telluride thin film solar cells. 2012 IEEE 38th Photovoltaic Specialists Conference (PVSC) PART 2, 2012, pp. 1–6, https://doi.org/10.1109/PVSC-Vol2.2012.6656778.

[6] M.O. Reese, C.L. Perkins, J.M. Burst, S. Farrell, T.M. Barnes, S.W. Johnston, D. Kuciauskas, T.A. Gessert, W.K. Metzger, Intrinsic surface passivation of CdTe, J. Appl. Phys. 118 (15) (2015) 155305, https://doi.org/10.1063/1.4933186.

[7] S. Tatarenko, F. Bassani, J.C. Klein, K. Saminadayar, J. Cibert, V.H. Etgens, Surface reconstructions of (001) CdTe and their role in the dynamics of evaporation and molecular-beam epitaxy growth, J. Vac. Sci. Technol. A 12 (1) (1994) 140–147, https://doi.org/10.1116/1.578910.

[8] B. Rerbal, G. Merad, H. Mariette, H. Faraoun, J.-M. Raulot, Ab initio investigation of the CdTe (001) surface, Superlattices Microstruct. 46 (5) (2009) 733–744, https://doi.org/10.1016/j.spmi.2009.07.025.

[9] R. Duszak, S. Tatarenko, J. Cibert, K. Saminadayar, C. Deshayes, (111) CdTe surface structure: a study by reflection high energy electron diffraction, x-ray photoelectron spectroscopy, and x-ray photoelectron diffraction, J. Vac. Sci. Technol. A 9 (6) (1991) 3025–3030, https://doi.org/10.1116/1.577167.

[10] H.R. Moutinho, R.G. Dhere, M.J. Romero, C.-S. Jiang, B. To, M.M. Al-Jassim, Electron backscatter diffraction of CdTe thin films: effects of $CdCl_2$ treatment, J. Vac. Sci. Technol. A 26 (4) (2008) 1068–1073, https://doi.org/10.1116/1.2841523.

[11] G. Stechmann, S. Zaefferer, P. Konijnenberg, D. Raabe, C. Gretener, L. Kranz, J. Perrenoud, S. Buecheler, A.N. Tiwari, 3-Dimensional microstructural characterization of CdTe absorber layers from CdTe/CdS thin film solar cells, Sol. Energy Mater. Sol. Cells 151 (2016) 66–80, https://doi.org/10.1016/j.solmat.2016.02.023.

[12] W. Orellana, E. Menéndez-Proupin, M.A. Flores, Self-compensation in chlorine-doped CdTe, Sci. Rep. 9 (2019) 9194, https://doi.org/10.1038/s41598-019-45625-x.

[13] S. Smidstrup, T. Markussen, P. Vancraeyveld, J. Wellendorff, J. Schneider, T. Gunst, B. Verstichel, D. Stradi, P.A. Khomyakov, U.G. Vej-Hansen, M.-E. Lee, S. T. Chill, F. Rasmussen, G. Penazzi, F. Corsetti, A. Ojanper, K. Jensen, M.L. N. Palsgaard, U. Martinez, A. Blom, M. Brandbyge, K. Stokbro, QuantumATK: an integrated platform of electronic and atomic-scale modelling tools, J. Phys.: Condens. Matter 32 (1) (2019) 015901, https://doi.org/10.1088/1361-648x/ab4007.

[14] QuantumATK Q-2019.12, Synopsys QuantumATK.

[15] A.P. Nicholson, U. Martinez, A. Shah, A. Thiyagarajan, W.S. Sampath, Atomistic modeling of energy band alignment in CdTe(100) and CdTe(111) surfaces, Appl. Surf. Sci. 528 (2020) 146832, https://doi.org/10.1016/j.apsusc.2020.146832.

[16] D. Martrou, J. Eymery, N. Magnea, Equilibrium shape of steps and islands on polar II-VI semiconductors surfaces, Phys. Rev. Lett. 83 (1999) 2366–2369, https://doi.org/10.1103/PhysRevLett.83.2366.

[17] T. Ozaki, Variationally optimized atomic orbitals for large-scale electronic structures, Phys. Rev. B 67 (2003) 155108, https://doi.org/10.1103/PhysRevB.67.155108.

[18] T. Ozaki, H. Kino, Numerical atomic basis orbitals from H to Kr, Phys. Rev. B 69 (2004) 195113, https://doi.org/10.1103/PhysRevB.69.195113.

[19] J.P. Perdew, A. Zunger, Self-interaction correction to density-functional approximations for many-electron systems, Phys. Rev. B 23 (1981) 5048–5079, https://doi.org/10.1103/PhysRevB.23.5048.

[20] S. Smidstrup, D. Stradi, J. Wellendorff, P.A. Khomyakov, U.G. Vej-Hansen, M.-E. Lee, T. Ghosh, E. Jónsson, H. Jónsson, K. Stokbro, First–principles Green's-function method for surface calculations: a pseudopotential localized basis set approach, Phys. Rev. B 96 (2017) 195309, https://doi.org/10.1103/PhysRevB.96.195309.

[21] A. Romeo, Chapter I-3-B - CdTe Solar Cells, in: S.A. Kalogirou (Ed.), McEvoy's Handbook of Photovoltaics, 3rd, Academic Press, 2018, pp. 309–369, https://doi.org/10.1016/B978-0-12-809921-6.00009-4.

[22] G. Srivastava, The electron counting rule and passivation of compound semiconductor surfaces, Appl. Surf. Sci. 252 (21) (2006) 7600–7607, https://doi.org/10.1016/j.apsusc.2006.03.076.Proceedings of the 4th International Workshop on Semiconductor Surface Passivation

[23] J.D. Benson, B.K. Wagner, A. Torabi, C.J. Summers, Surface stoichiometry and reaction kinetics of molecular beam epitaxially grown (001)CdTe surfaces, Appl. Phys. Lett. 49 (16) (1986) 1034–1036, https://doi.org/10.1063/1.97463.

[24] P. Lu, D.J. Smith, Direct imaging of CdTe(001) surface reconstructions by high-resolution electron microscopy, Surf. Sci. 254 (1) (1991) 119–124, https://doi.org/10.1016/0039-6028(91)90644-8.

[25] C. Heske, U. Winkler, H. Neureiter, M. Sokolowski, R. Fink, E. Umbach, C. Jung, P. R. Bressler, Preparation and termination of well-defined CdTe(100) and Cd(Zn)Te (100) surfaces, Appl. Phys. Lett. 70 (8) (1997) 1022–1024, https://doi.org/10.1063/1.118432.

[26] P. Brown, K. Durose, G.J. Russell, J. Woods, The absolute determination of CdTe crystal polarity, J. Cryst. Growth 101 (1) (1990) 211–215, https://doi.org/10.1016/0022-0248(90)90968-Q.

[27] C.K. Egan, Q.Z. Jiang, A.W. Brinkman, Morphology and reconstructions of polar CdTe(111)A,B surfaces by scanning tunneling microscopy, J. Vac. Sci. Technol. A 29 (1) (2011) 011021, https://doi.org/10.1116/1.3525914.

[28] D. Cahen, A. Kahn, Electron energetics at surfaces and interfaces: concepts and experiments, Adv. Mater. 15 (4) (2003) 271–277, https://doi.org/10.1002/adma.200390065.

[29] L.J. Brillson, Adsorbates on Electronic Materials' Surfaces, John Wiley & Sons, Ltd, pp. 327–363. 10.1002/9783527665709.ch18.

[30] R.T. Tung, Recent advances in schottky barrier concepts, Mater. Sci. Eng. 35 (1) (2001) 1–138, https://doi.org/10.1016/S0927-796X(01)00037-7.

[31] R. Cohen, S. Bastide, D. Cahen, J. Libman, A. Shanzer, Y. Rosenwaks, Controlling electronic properties of CdTe by adsorption of dicarboxylic acid derivatives: relating molecular parameters to band bending and electron affinity changes, Adv. Mater. 9 (9) (1997) 746–749, https://doi.org/10.1002/adma.19970090915.

[32] A. Haddout, A. Raidou, M. Fahoume, Influence of the layer parameters on the performance of the CdTe solar cells, Optoelectron. Lett. 14 (2018) 98–103, https://doi.org/10.1007/s11801-018-7229-4.

[33] J. Kephart, J. McCamy, Z. Ma, A. Ganjoo, F. Alamgir, W. Sampath, Band alignment of front contact layers for high-efficiency CdTe solar cells, Sol. Energy Mater. Sol. Cells 157 (2016) 266–275, https://doi.org/10.1016/j.solmat.2016.05.050.

[34] S. Demtsu, J. Sites, Effect of back-contact barrier on thin-film CdTe solar cells, Thin Solid Films 510 (1) (2006) 320–324, https://doi.org/10.1016/j.tsf.2006.01.004.